A Novel Handling Method to Intermittent Feedback in Load Frequency Regulation for Renewable Energy-Dominated Microgrids

Zhijian Hu, Qingyang Li, Pu Zhang, Ruiping Wang, Kai Zhang

A Novel Handling Method to Intermittent Feedback in Load Frequency Regulation for Renewable Energy-Dominated Microgrids

Zhijian Hu, *Member, IEEE*, Qingyang Li, Pu Zhang, *Member, IEEE*, Ruiping Wang, and Kai Zhang

***Abstract*—Traditional thermal-based microgrids are transforming towards distributed renewable energy sources (DRESs) dominated microgrids, aiming at promoting sustainable environment and economy. This work thus incorporates two popular DRESs (i.e., wind turbines and plug-in electric vehicles (PEVs)) in the thermal-based power plants. Considering the inevitable sensor failures caused by hostile outdoor environment and the communication failures caused by resource constraints, this paper proposes a novel handling method to intermittent feedback in load frequency control (LFC) for microgrids. Furthermore, to deal with the fluctuations of power outputs from DRESs, this paper incorporates the robust performance index into the control law derivation. By taking into account such intermittent feedback and robust performance index, the operation of microgrid system can better realize resiliency enhancement. Validation results demonstrate the feasibility of this novel handling method under different degree of intermittent feedback.**

***Index Terms*—Intermittent measurement, microgrid, load frequency control, wind turbine, plug-in electric vehicle.**

I. Introduction

Growing climate changes put forward higher requirements to energy sectors to promote sustainable development and decarbonization. Increasing the penetration level and the diversity of distributed renewable energy sources (DRESs) into the traditional thermal-based microgrids becomes a promising solution [1], [2]. While, with the increasing penetration of DRESs, the physical inertia of power systems, traditionally provided by synchronous generators, reduces sharply. This incurs greater challenges to frequency stability guarantees. Furthermore, the renewable power outputs of DRESs are fluctuant due to the uncertainties of natural resources, such as the stochastic wind speed. As a result, this paper aims to incorporate multiple DRESs, and in this context, propose a robust frequency controller to reduce the influence of DRESs power output fluctuation on frequency stability

Among DRESs, the wind power generation has emerged as a most critical contributor to promote the green energy exploration, as of the most recent assessments in 2023 [3]. The modular scalability of wind farms, coupled with advancements in turbine technology and economies of scale, has contributed to the increasing cost-effectiveness of wind energy. Research and development initiatives have furthered the understanding of wind dynamics [4], aiding in advancing wind turbine control technologies for stable wind power harvesting. Despite notable progress has been made to understand the wind turbine model and the wind power profile, the application challenges such as fluctuant power output and grid integration persist, necessitating the effectiveness explorations of existing control methodologies in real-world scenarios.

For load frequency control (LFC) design at the microgrid level, consecutive feedback control signals are a prerequisite to ensure the frequency stability [5], [6]. On the one hand, due to the fact that smart sensors (e.g., the phase measurement units (PMUs) and remote telemetry units (RTUs)) are usually allocated in outdoor environment [7], they potentially suffer functional faults such as failed element, degraded processing capacity, and sensor aging. As a direct consequence of sensor faults, measurements from sensors are intermittent, which disable the LFC implementation with output feedback control techniques. On the other hand, modern microgrids prefer the wireless sensor network (WSN) to realize data sharing, during which process the communication link failure may occur [8]–[10]. However, existing results addressing multiple sources of intermittent feedback control signals within sensor-controller loop for LFC issues are limited. Considering the intermittent measurements from sensors, the authors in [11]–[19] revealed some effective solutions. From the perspective of modeling, the authors in [11] took into account PMU failures caused by disorder interaction between hardware and software and modeled this category of failures using a Markov model-based unified PMU reliability model, which greatly aided in the estimation of PMU failure data using the Monte Carlo simulation technique. The authors in [15] characterized PMU failure as a hidden Markov model and performed the reliability analysis of PMUs, based on which the transient probability is computed,

This work is supported in part by the European Union's Horizon 2022 Research and Innovation Programme for the Marie Skłodowska-Curie Actions under Grant 101108472, in part by National Natural Science Foundation of China under Grant 62203142, in part by Aeronautical Science Foundation of China under Grant 2022Z071077009, and in part by New Era-Longjiang Excellent Master and Ph.D Thesis Funding Project under Grant LJYXL2022-008. (*Corresponding author: Kai Zhang.*)

Z. Hu is with LAAS-CNRS, Université de Toulouse, CNRS, Toulouse 31400, France and also with the School of Electrical and Electronic Engineering, Nanyang Technological University, 639798, Singapore (e-mail: huzhijian1991@gmail.com).

Q. Li is with the School of Electrical Engineering, Harbin Institute of Technology, Harbin 150001, China (e-mail: qingyangli0905@gmail.com).

P. Zhang is with the School of Automation and Information Engineering, Xi'an University of Technology, Xi'an 710048, China (e-mail: zhangpu@xaut.edu.cn).

R. Wang is with the School of Computer Science and Engineering, Nanyang Technological University, 639798, Singapore (e-mail: ruiping.wang@ntu.edu.sg).

K. Zhang is with the School of Instrument Science and Engineering, Harbin Institute of Technology, Harbin 150001, China and also with Department of Biomedical Engineering, City University of Hong Kong, Hong Kong (e-mail: kaizhang0116@163.com).

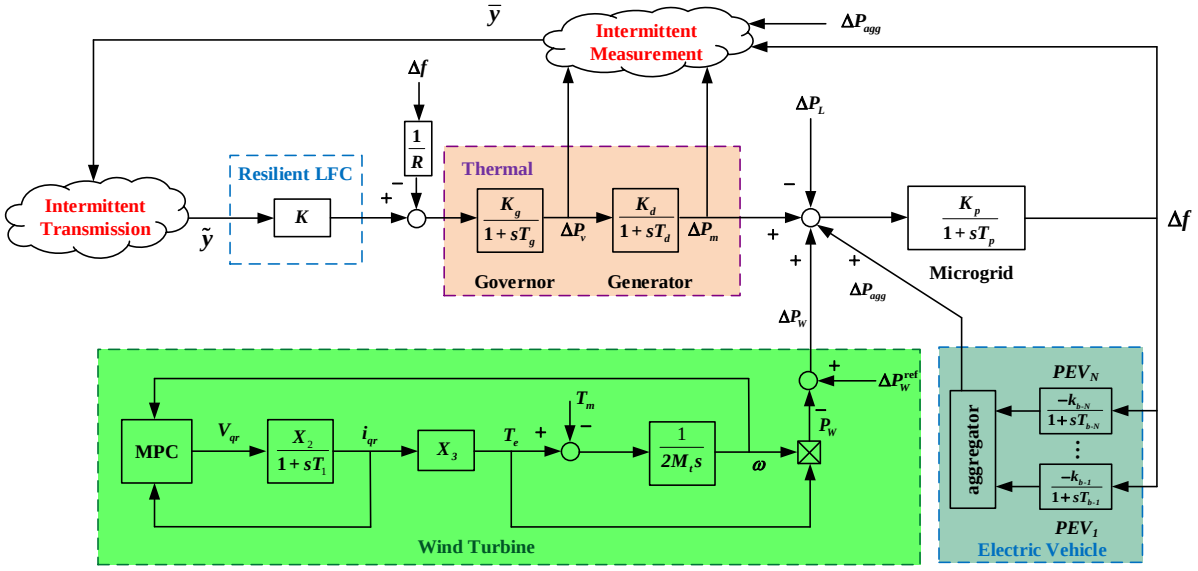

Fig. 1. Schematic of resilient LFC with intermittent feedback signals.

leading to improved transient states monitoring to enable quick restorative initiatives. Considering the intermittent transmission caused by unreliable communication links, the authors in [20] proposed a hybrid rapid path recovery technique to lessen the effects of signal communication channel failures. While the authors in [21] argued that the intermittent transmission can be a consequence of denial-of-service attacks, and in this context they tackled the decentralized LFC problem by resorting to an aperiodic sampled-data control method. To the best knowledge of the authors, till now few of existing results revealed a systematic method for LFC by simultaneously addressing the intermittent measurements from sensors and the intermittent transmissions over communication networks, though it is a hidden hazard in practical engineering.

Based on above discussion, this work endeavors to present a novel handling method to intermittent feedback signals for LFC of renewable energy-dominated microgrids. This novel handling method is capable of explaining and handling both the intermittent measurement from PMUs and the intermittent transmission over communication networks. The schematic of the proposed method is illustrated in Fig. 1. The main contributions are listed in what follows:

- Compared to the results revealed in [11]–[21], the proposed handling method to intermittent feedback signals generally addresses both the intermittent measurement and the intermittent transmission. Two theorems are derived to guarantee the existence and solvability of the proposed method, with the robust performance index incorporated in the stability analysis and control synthesis.
- To mitigate the impact of fluctuant power output from DRESs on system stability, a hierarchical LFC framework is presented. At the low-level DRESs integration, the MPC policy is adopted to track the assigned power. At the high-level LFC, the resilient controller is designed considering the intermittent feedback signals.
- To address the potential change of the steady state operating point of microgrids due to fluctuant renewable power integration, this work advances the commonly used LFC models [21], [22] by incorporating an unknown but bounded matrix, which can well tolerant the change of system parameters and extend the applicability of traditional linearized LFC models.
- To speed up the frequency dynamic, plug-in electric vehicles (PEVs) are aggregated as an additional power supply to participate the LFC considering the battery's fast charging/discharging capabilities, which expands the application scope of the results in [23]–[25].

The remaining work is structured as below. Section II designs an MPC policy for rated wind power tracking. Section III develops the LFC model with PEV participation and proposes two theorems capable to guarantee the existence and solvability of the resilient controller with intermittent feedback signals. Section IV verifies the rapidity of frequency dynamic with PEV participation and the resiliency of the proposed controller under different level of intermittent feedback signals. Section V summarizes the work.

II. Rated Wind Power Tracking under MPC

A. Modeling of Wind Turbines

Due to the simple implementation in either offshore or onshore settings, the exploration of wind energy has experienced a significant increase among various categories of DRESs in recent years. This work thus gives a detailed discussion on wind turbine modeling, followed by the MPC policy. As for other categories of DRESs, we no longer discuss in detail but mimic the profile of fluctuant harvested power through random function in validations. A simplified double fed induction generator model [26] is adopted, see Fig. 1, and the system

dynamics is described as

$$\dot{i}_{qr} = -\left(\frac{1}{T_1}\right) i_{qr} + \left(\frac{X_2}{T_1}\right) V_{qr}, \tag{1}$$

$$\dot{\omega} = -\left(\frac{X_3}{2M_t}\right) i_{qr} + \left(\frac{1}{2M_t}\right) T_m, \tag{2}$$

where $X_2 = 1/R_r$, $X_3 = L_m/L_{ss}$, $T_1 = L_0/(\omega_s R_s)$, $T_e = X_3 i_{qr}$, $L_0 = L_{rr} + L_m^2/L_{ss}$, $L_{ss} = L_s + L_m$, $L_{rr} = L_r + L_m$; ω is the rotational speed; T_m is the mechanical torque; $P_W = \omega T_e$ is the active power output; i_{qr} and V_{qr} are the q-axial rotor current and voltage; meanings of other parameters in (1) and (2) can be found in [26].

By choosing $x_W = [i_{qr} \quad \omega]^T$, (1) and (2) can be formulated as

$$\begin{cases} \dot{x}_W = \mathscr{A}_{\mathscr{W}} x_W + \mathscr{B}_{\mathscr{W}} u_W + \mathscr{F}_{\mathscr{W}} v_W, \\ y_W = \mathscr{C}_{\mathscr{W}} x_W, \end{cases} \tag{3}$$

where $u_W = V_{qr}$ is the control action; $v_W = T_m$ is the electromagnetic disturbance; y_W is the measurement with $\mathscr{C}_W = I_2$;

$$\mathscr{A}_{\mathscr{W}} = \begin{bmatrix} \frac{-1}{T_1} & 0 \\ \frac{-X_3}{2M_t} & 0 \end{bmatrix}, \mathscr{B}_{\mathscr{W}} = \begin{bmatrix} \frac{X_2}{T_1} \\ 0 \end{bmatrix}, \mathscr{F}_{\mathscr{W}} = \begin{bmatrix} 0 \\ \frac{1}{2M_t} \end{bmatrix}.$$

In view that the state measurements of wind power generation systems are usually realized by digital sensors to facilitate the control design, (3) is discretized to

$$x_W(k+1) = A_W x_W(k) + B_W u_W(k) + F_W v_W(k), \tag{4}$$

$$y_W(k) = C_W x_W(k), \tag{5}$$

where $A_W = e^{\mathscr{A}_{\mathscr{W}} l}$, $B_W = \int_0^l e^{\mathscr{A}_{\mathscr{W}} l} \mathscr{B}_{\mathscr{W}} dl$, $C_W = \mathscr{C}_{\mathscr{W}}$, and $F_W = \int_0^l e^{\mathscr{A}_{\mathscr{W}} l} \mathscr{F}_{\mathscr{W}} dl$; l is the sampling period.

B. MPC Formulation

To actualize the assigned power tracking from wind turbines, this work employs the MPC policy, a most promising approach in microgrids due to its superiority in solving finite-horizon constrained optimization problems at each sampling instant. The cost function of the MPC is chosen as

$$\mathcal{J}(\boldsymbol{x_W}(k), \boldsymbol{u_W}(k)) = \sum_{m=0}^{\bar{M}-1} (\|x_W(k+m|k) - x_W^{\text{ref}}\|_Q^2 + \|u_W(k+m|k) - u_W^{\text{ref}}\|_S^2) + V_f(x_W(k+\bar{M}|k)) \tag{6}$$

where $\boldsymbol{u_W}(k) = [u_W(k|k)^T \quad u_W(k+1|k)^T \quad \cdots \quad u_W(k+\bar{M}-1|k)^T]^T$, and $\boldsymbol{x_W}(k) = [x_W(k+1|k)^T \quad x_W(k+2|k)^T \quad \cdots \quad x_W(k+\bar{M}|k)^T]^T$; $V_f = x_W(k+\bar{M}|k)^T P x_W(k+\bar{M}|k)$ is the terminal cost related to system stability; $\bar{M}$ defines the prediction (control) horizon; x_W^{ref} is the reference of x_W; u_W^{ref} is the reference of u_W; $k+m \mid k$ means the predicted value at time $k+m$ with the real-time measurements at time k; $Q \succ 0$ and $S \succeq 0$ are two tunning matrices. The selection of control and prediction horizons necessitates a careful balance between tracking accuracy and computational constraints. To enhance the tracking precision and effective disturbance rejection, a longer prediction horizon is advisable. However, this increases computational complexity, potentially impeding real-time implementation. Therefore, it is imperative to ensure that the selected prediction horizon does not introduce undue delays. Besides, the control horizon should be appropriately set to be shorter than the prediction horizon, optimizing computational efficiency while maintaining control performance.

The MPC approach can well address states constraints during the process of seeking for optimal control actions. For wind power generation systems, the constraints mainly refer to current, rotational speed, stator/rotor side converters. Considering these constraints, a formal MPC policy for assigned power tracking is

$$\min_{\boldsymbol{u_W}} \mathcal{J}(\boldsymbol{x_W}(k), \boldsymbol{u_W}(k))$$

$$\text{s.t.} \begin{cases} x_W(k+m+1|k) = A_W x_W(k+m|k) \\ \qquad\qquad + B_W u_W(k+m|k), \\ x_W(k|k) = x_W(k), \\ x_W(k+\bar{M}|k) \in \Omega, \\ i_{qr,\min} \le i_{qr}(k+m|k) \le i_{qr,\max}, \\ \omega_{\min} \le \omega(k+m|k) \le \omega_{\max}, \\ m = 0, 1, 2, \cdots, \bar{M}-1, \end{cases} \tag{7}$$

where Ω is the terminal region constraint; $i_{qr,\min}(i_{qr,\max})$ and $\omega_{\min}(\omega_{\max})$ are the lower (upper) bounds of i_{qr} and i_{qr}.

III. Resilient LFC Considering Intermittent Feedback Signals

A. Modeling of PEVs

The power source of PEVs is the battery, which is typically constituted by a multitude of interconnected battery cells. They establish a connection with the power grid through a DC/AC converter [27]. For integration with the power grid, the equivalent circuit is shown in Fig. 2(a), where I_{dc} and V_{dc} represent the battery's DC current and voltage, and P_{V2G} signifies the active power injected into the power grid via the vehicle-to-grid infrastructure.

Corresponding to Fig. 2(b), the system dynamics of the battery are represented by

$$-\frac{V_{boc} + V_{\text{dc}} + V_b}{R_{\text{bc}}} = I_{\text{dc}}, \tag{8}$$

$$C_{bp}\frac{dV_{boc}}{dt} + \frac{V_{boc}}{R_{bp}} = I_{\text{dc}}, \tag{9}$$

$$C_b\frac{dV_b}{dt} + \frac{V_b}{R_b} = I_{\text{dc}}, \tag{10}$$

where V_{boc} denotes the open circuit voltage; V_b signifies the overvoltage; R_{bp} represents the resistance of self discharging; R_b and C_b account for the transient overvoltage effects; C_{bp} means the capacitance; and R_{bc} stands for the resistance related to the terminals and inter-cell connections of the battery.

By ignoring the power loss of the equivalent circuit, the power supplied to the grid is identical to that generated by the battery, which can be represented by

$$P_{V2G} = P_{dc} = I_{dc} V_{dc}. \tag{11}$$

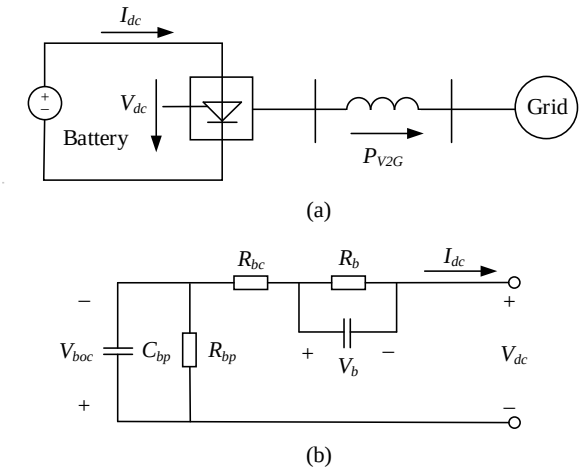

Fig. 2. PEV model [27]. (a) PEV's equivalent circuit; (b) Battery's equivalent circuit.

By neglecting the higher-order components, the increment of V2G power from (11) is calculated by

$$\Delta P_{V2G} = V_{dc}^0 \Delta I_{dc} + I_{dc}^0 \Delta V_{dc}, \tag{12}$$

where $\Delta V_{dc} = V_{dc} - V_{dc}^0$, $\Delta I_{dc} = I_{dc} - I_{dc}^0$; and V_{dc}^0 and I_{dc}^0 signify the original values of V_{dc} and I_{dc}^0.

Through dividing the DC voltage into two elements as

$$\Delta V_{dc} = \Delta V_r + \Delta V_s, \tag{13}$$

we can ultimately arrive at

$$\Delta P_{V2G} = V_{dc}^0 \Delta I_{dc} + I_{dc}^0 \left(\Delta V_r + \Delta V_s\right). \tag{14}$$

In light of the compensation aspect as explicated by the authors in [28], an incremental adjustment of the battery voltage is incorporated as a corrective measure to mitigate power fluctuations arising from deviations in current. Consequently, the term $I_{dc}^0 \Delta V_r$ in (14) is specifically allocated for power compensation to alterations in ΔI_{dc}. Concurrently, the term $I_{\mathrm{dc}}^0 \Delta V_s$ in (14) is attributed to the accommodation of V2G power in response to LFC. Subsequently, we have

$$\Delta P_{V2G} = I_{dc}^0 \Delta V_s. \tag{15}$$

Within LFC, ΔV_s is meticulously modulated in response to variations in frequency, thereby yielding

$$\Delta \dot{V}_s = \frac{1}{T_b}\left(-\Delta V_s - k_v \Delta f\right). \tag{16}$$

As a result, the V2G power that one PEV contributes to LFC is

$$\Delta \dot{P}_{V2G} = \frac{1}{T_b}\left(-\Delta P_{V2G} - K_b \Delta f\right). \tag{17}$$

where K_b and T_b indicate the gain and the time constant of a battery; and $K_b = k_v I_{dc}^0$.

In real-world scenarios, an individual PEV can hardly participate in LFC due to the limited power capacity of the battery. Therefore, an aggregator, functioning as an intermediate agent between the PEVs and the grid, is usually employed to aggregate the grid-scale power capacity for LFC from thousands of PEVs. As for the aggregation algorithm design, interested readers can refer to our previous work [29], where we proposed a maximal power acquisition algorithm tailored for PEV remaining capacity aggregation. To focus on the resilient LFC design under intermittent feedback signals, this work concisely substitutes ΔP_{V2G} by ΔP_{agg} in the following discussion.

B. Modeling of Microgrids

The microgrid employed in this work (see Fig. 1) is made up of generator dynamic, governor dynamic, and microgrid dynamic. The system dynamics are described as

$$\Delta \dot{P}_m = -\frac{1}{T_d}\Delta P_m + \frac{K_d}{T_d}\Delta P_v, \tag{18}$$

$$\Delta \dot{P}_v = -\frac{K_g}{RT_g}\Delta f - \frac{1}{T_g}\Delta P_v + \frac{K_g}{T_g}\Delta P_c, \tag{19}$$

$$\begin{aligned}\Delta \dot{f} = &-\frac{1}{T_p}\Delta f + \frac{K_p}{T_p}\Delta P_m + \frac{K_p}{T_p}\Delta P_W - \frac{K_p}{T_p}\Delta P_L \\ &+ \frac{K_p}{T_p}\Delta P_O + \frac{K_p}{T_p}\Delta P_{agg},\end{aligned} \tag{20}$$

where K_g, K_d, and K_p denote the governor, generator, and microgrid gains; ΔP_W denotes the wind power deviation; ΔP_O indicates the total deviations caused by other DRESs; other parameters are defined in [18].

Notably, (17)-(20) constitute the small-signal model for LFC by linearizing the power generation system around one steady-state operating point, wherein system parameters are only accurate for small load disturbances. For the multi-energy systems, the linearized system parameters may not always precise because of the potential movement of the steady-state operating point because of fluctuant power outputs from DRESs. To advance [22] where only the uncertainty on R is addressed, the paper addresses more general parameter uncertainties and describes them by incorporating an unknown and bounded matrix $\Delta\mathscr{A}(t)$ to the existing small-signal model, which is capable to address all parameter uncertainties. Thus, the improved small-signal model for (17)-(20) becomes

$$\begin{cases} \dot{x} = (\mathscr{A} + \Delta\mathscr{A}(t))x + \mathscr{B}u + \mathscr{F}v, \\ y = \mathscr{C}x, \end{cases} \tag{21}$$

where $x = [\Delta f \quad \Delta P_m \quad \Delta P_v \quad \Delta P_{agg}]^T$, $\mathscr{C} = I_3$, $u = \Delta P_c$; $v = [\Delta P_W \quad \Delta P_O \quad \Delta P_L]^T$, $v \in l_2[0,\infty)$ is generally seen as the load disturbance; $\Delta\mathscr{A}(t)$ is an unknown and time-

varying matrix to explain the parameter change; and

$$\mathscr{A}=\begin{bmatrix} \frac{-1}{T_p} & \frac{K_p}{T_p} & 0 & \frac{1}{T_p} \\ 0 & \frac{-1}{T_d} & \frac{K_d}{T_d} & 0 \\ \frac{-K_g}{RT_g} & 0 & \frac{-1}{T_g} & 0 \\ \frac{-K_b}{T_b} & 0 & 0 & \frac{-1}{T_b} \end{bmatrix},$$

$$\mathscr{F}=\begin{bmatrix} \frac{K_p}{T_p} & \frac{-K_p}{T_p} & \frac{K_p}{T_p} \\ 0 & 0 & 0 \\ 0 & 0 & 0 \\ 0 & 0 & 0 \end{bmatrix}, \mathscr{B}=\begin{bmatrix} 0 \\ 0 \\ \frac{K_g}{T_g} \\ 0 \end{bmatrix}.$$

In LFC, all states are measured and transmitted by digital sensors, such as PMUs and RTUs. Hence, (21) is discretized by

$$\begin{cases} x(k+1)=(A+\Delta A(k))x(k)+Bu(k)+Fv(k), \\ y(k)=Cx(k), \end{cases} \tag{22}$$

where $A=e^{\mathscr{A}l}$, $B=\int_0^l e^{\mathscr{A}\tau}\mathscr{B}d\tau$, $C=\mathscr{C}$, $F=\int_0^l e^{\mathscr{A}\tau}\mathscr{F}d\tau$, and $\Delta A(k)=NG(k)Y$; l is the sampling time; N and Y are given matrices; $G(k)$ is assumed to be an unknown, time-varying, and Lebesgue measurable matrix satisfying $G^T(k)G(k)\preceq I$.

C. Control Formulation with Intermittent Feedback Signals

A typical output feedback law for LFC is adopted,

$$u(k)=K\tilde{y}(k), \tag{23}$$

where K is the controller gain to be determined, and $\tilde{y}(k)$ is the actual signal used in control formulation.

To formulate a more practical frequency controller, this work considers the intermittent feedback signals, include the intermittent measurement caused by temporary sensor failures and the intermittent transmission caused by unreliable communication networks. To model the temporary sensor failures, this work employs Bernoulli variable $\vartheta(k)$ [17], [18], which is able of capturing the intermittency extent by flexibly selecting various probability distributions. The actual measurement $\bar{y}(k)$ from the sensor is depicted by

$$\bar{y}(k)=\vartheta(k)y(k), \tag{24}$$

where $\text{Prob}\{\vartheta(k)=1\}=\bar{\vartheta}$, $\text{Prob}\{\vartheta(k)=0\}=1-\bar{\vartheta}$ with $\bar{\vartheta}\in[0,1]$ indicating the probability that the signal $y(k)$ is accurately measured, and $\text{Prob}\{\cdot\}$ indicating the probability operator.

To model the intermittent transmission caused by unreliable communication networks, the Bernoulli variable $\varrho(k)$ is adopted. The practically transmitted signal to the control center is depicted as

$$\tilde{y}(k)=\varrho(k)\bar{y}(k), \tag{25}$$

where $\text{Prob}\{\varrho(k)=1\}=\bar{\varrho}$, $\text{Prob}\{\varrho(k)=0\}=1-\bar{\varrho}$ with $\bar{\varrho}\in[0,1]$ representing the probability that the measurement is successfully transmitted from sensor side to the controller side.

By taking (23)-(25) to (22), the closed-loop LFC model is deduced as,

$$x(k+1)=(A+\Delta A(k)+\vartheta(k)\varrho(k)BKC)x(k)+Fv(k). \tag{26}$$

D. Stability Analysis

To promote the control law derivation, we propose Theorem 1. Based on the sufficient condition therein, we can automatically calculate the resilient controller gains by resorting to the mincx solver in linear matrix inequality toolbox (LMI) in Matlab.

Theorem 1: Considering the intermittent measurement probability $\bar{\vartheta}$ and the intermittent transmission probability $\bar{\varrho}$, the system (26) is mean-square asymptotically stable with Δf satisfying the predefined $\mathcal{H}_\infty$ index γ if there exists matrix $P\succ 0$, such that

$$\begin{bmatrix} \tilde{\Omega}+D^TD & \tilde{A}^TPF \\ \star & F^TPF-\gamma^2I \end{bmatrix}\prec 0, \tag{27}$$

where $\tilde{\Omega}=\tilde{A}^TP\tilde{A}+\tilde{B}^TP\tilde{B}-P$, $\tilde{B}=\sqrt{\bar{\vartheta}\bar{\varrho}(1-\bar{\vartheta}\bar{\varrho})}BKC$, $\tilde{A}=A+\Delta A(k)+\bar{\vartheta}\bar{\varrho}BKC$, and $D=\text{diag}\{1,0,0,0\}$ with $\text{diag}\{\cdot\}$.

Proof: By choosing the following Lyapunov function

$$V(k)=x^T(k)Px(k),$$

one can derive

$$\begin{aligned} \Delta V(k)=&\mathcal{E}\{[x^T(k)(\tilde{A}+(\vartheta(k)\varrho(k)-\bar{\vartheta}\bar{\varrho})BKC)^T \\ &+v^T(k)F^T]P[(\tilde{A}+(\vartheta(k)\varrho(k)-\bar{\vartheta}\bar{\varrho})BKC)x(k) \\ &+Fv(k)]\}-x^T(k)Px(k) \\ =&\begin{bmatrix} x(k) \\ v(k) \end{bmatrix}^T\begin{bmatrix} \tilde{\Omega} & \tilde{A}^TPF \\ \star & F^TPF \end{bmatrix}\begin{bmatrix} x(k) \\ v(k) \end{bmatrix}. \end{aligned}$$

with $\mathcal{E}\{\cdot\}$ indicating the mathematical expectation.

When there is no disturbance, we have

$$\Delta V(k)=x^T(k)\tilde{\Omega}x(k). \tag{28}$$

According to (27), one can derive $\Delta V(k)<0$ for all $x(k)\neq 0$, leading to $\lim_{k\to\infty}\mathcal{E}\{\|x(k)\|\}=0$. Consequently, system (26) is mean-square stable [30].

When there are some disturbances, one defines the following function.

$$\Phi(k)=\Delta V(k)-\gamma^2v^T(k)v(k)+\Delta f^T(k)\Delta f(k). \tag{29}$$

Through summing the expectation of each side of (29) from $k=0$ to $k=\infty$, one arrives

$$\begin{aligned} \tilde{\Phi}=&\mathcal{E}\Big\{\sum_{k=0}^{\infty}\Phi(k)\Big\} \\ =&\mathcal{E}\{V(\infty)\}-V(0)+\mathcal{E}\Big\{\sum_{k=0}^{\infty}\Delta f^T(k)\Delta f(k)\Big\} \\ &-\gamma^2\sum_{k=0}^{\infty}v^T(k)v(k). \end{aligned}$$

Based on the sufficient condition (27), one arrives $\tilde{\Phi} < 0$. Furthermore, $\mathcal{E}\{V(\infty)\} \geq 0$. As a result, if $V(0) = 0$, then $\|\Delta f\|_{\mathcal{E}_2}^2 < \gamma^2 \|v\|_2^2$ establishes for all nonzero $v \in l_2[0, \infty)$. Therefore, Δf satisfies the prescribed $\mathcal{H}_\infty$ performance index γ [30]. The proof of Theorem 1 is completed. ■

E. Control Synthesis

The presented condition (27) poses challenges for solution using the LMI toolbox in Matlab, primarily due to two distinct reasons. Firstly, the coupling between the resilient controller gain K and the Lyapunov matrix P within (27) renders traditional LMI methods inadequate. Secondly, (27) contains a matrix $\Delta A(k)$ that is both time-varying and unknown. Consequently, to enable the automated determination of the resilient controller gain K from (27), we introduce Theorem 2. Theorem 2 is specifically devised to address the aforementioned challenges, decoupling K and P, and in the meantime, accommodating the complexities associated with the time-varying and unknown matrix $\Delta A(k)$.

Theorem 2: Considering the intermittent measurement probability $\bar{\vartheta}$ and the intermittent transmission probability $\bar{\varrho}$, the system (26) is mean-square asymptotically stable with Δf satisfying the predefined $\mathcal{H}_\infty$ index γ, if there exist matrices $P \succ 0$, $\bar{P} \succ 0$, and a scalar $\varsigma > 0$, such that

$$\begin{bmatrix} -\bar{P} & 0 & \tilde{B} & 0 & 0 \\ \star & -\bar{P} & A + \bar{\vartheta}\bar{\varrho}BKC & F & N \\ \star & \star & D^T D - P + \varsigma Y^T Y & 0 & 0 \\ \star & \star & \star & -\gamma^2 I & 0 \\ \star & \star & \star & \star & -\varsigma I \end{bmatrix} \prec 0, \tag{30}$$

$$P\bar{P} = I, \tag{31}$$

Proof: Utilizing Schur complement, Young's inequality, and Schur complement to (30), one arrives at

$$\begin{bmatrix} \bar{\Omega} + D^T D & \tilde{A}^T \bar{P}^{-1} F \\ * & F^T Z^{-1} F - \gamma^2 I \end{bmatrix} \prec 0, \tag{32}$$

where $\bar{\Omega} = \tilde{A}^T \bar{P}^{-1} \tilde{A} + \tilde{B}^T Z \bar{P}^{-1} \tilde{B} - P$.

Through defining $\bar{P} = P^{-1}$, one obtains (27). The proof of Theorem 2 is completed. ■

IV. Results

A. System Parameters

Parameters of the multi-energy microgrid and the resilient controller are given as [26]: $P_W^{\text{ref}} = 2MW$, corresponding to $i_{qr} = 1.75A$, and $\omega = 1.17rad/s$; $R_r = 0.00552pu$, $R_s = 0.00491pu$, $L_s = 0.09273pu$, $L_m = 3.96545pu$, $L_r = 0.1pu$, $M_t = 4.5s$, $l = 1s$, $Q = I_2$, $S = I_1$, $M = 5$, $K_d = 1$, $K_g = 1$, $K_p = 10$, $K_b = 11$, $T_b = 0.05$, $T_d = 1.2s$, $T_g = 0.1s$, $T_p = 20s$, $R = 0.06$, $N = [0.02; 0.02; 0.02; 0.02]$, $Y = N^T$, $G(k) = 0.1\sin(10k)$, $h = 1s$, $\gamma = 2$, $T_m(k) = 0.02e^{-0.01k}(\text{rand} - 0.5)$ with "rand" meaning a uniform-distributed random number belonging to [0,1], $\Delta P_O = 0.05e^{-0.01k}(\text{rand} - 0.5)$, and $\Delta P_L = 0.01e^{-0.01k}(\text{rand} - 0.5)$.

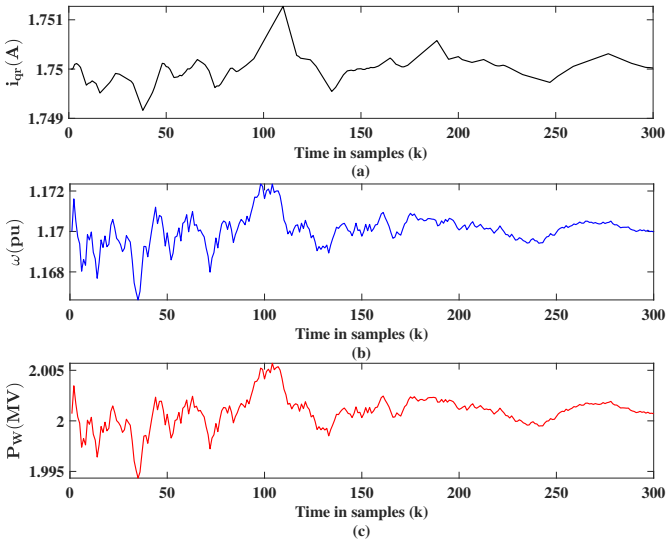

Fig. 3. Dynamics of wind power. (a) i_{qr}. (b) ω. (c) P_W.

B. Validations on Rated Wind Power Tracking under MPC

The dynamics of i_{qr} and ω for wind energy generation are depicted in Fig. 3(a)(b), respectively. As seen in Fig. 3(a)(b), the mechanical torque T_m disturbance causes both i_{qr} and ω to fluctuate around their reference values ($1.75A$ and $1.17rad/s$). Fig. 3(c) shows the dynamic of P_W combined with a substantially greater variation with an amplitude of $0.006MW$. Given that P_W is the product of ω, $X_3, and i_{qr}$, it is reasonable. By simply calculating $\Delta P_W = P_W - P_W^{\text{ref}}$, we can obtain the amplitude of wind power fluctuation, which is a kind of disturbance whose impact will be analyzed in Section IV.D.

C. Validations on Fast LFC with PEVs Participation

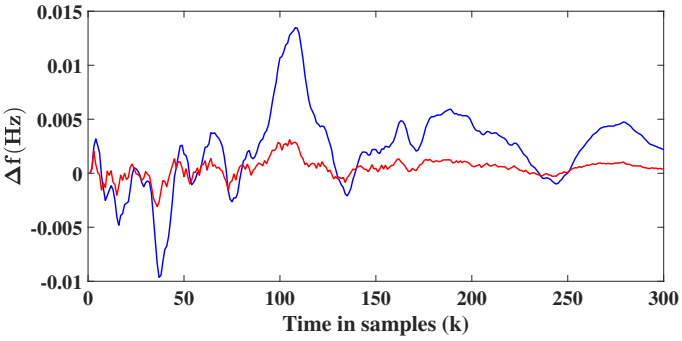

Fig. 4. Δf without and with PEVs. The blue line represents without PEVs. The red line represents with PEVs.

This section presents a comparative assessment of LFC with and without the participation of PEVs, using ideal feedback signals. Fig. 4 illustrates the frequency deviation dynamics for both scenarios. The controller gains for the scenario without the PEV participation are $[14.4248 \quad 0.4492 \quad -0.0163]$, which are automatically determined using the LMI toolbox without considering the PEV in the state

vector. While the gains with the PEV participation are $[-1.5279 \quad 0.3438 \quad 0.0372 \quad -0.0420]$, and these gains are automatically selected using the LMI toolbox based on Theorem 2. The results depicted in Fig. 4 clearly demonstrate that the inclusion of PEVs can significantly mitigate the overshoot of the frequency deviation curve compared to the scenario without the PEV participation. This reduction highlights the efficacy of PEVs in enhancing fast frequency regulation. The improvement can be attributed to the rapid charging and discharging capabilities of PEV batteries, which facilitate swift adjustments to frequency deviations.

D. Validations on Resilient LFC Considering Intermittent Feedback Signals

To demonstrate the merits of the proposed handling method to intermittent feedback signals, the conventional controller which does not consider the intermittency of the feedback signals is employed as the benchmark. The control gains of the conventional controller are automatically determined using the same methodological framework proposed in the resilient LFC strategy. This determination is executed through the LMI toolbox in Matlab, with the intermittency probability of the feedback signals set to zero.

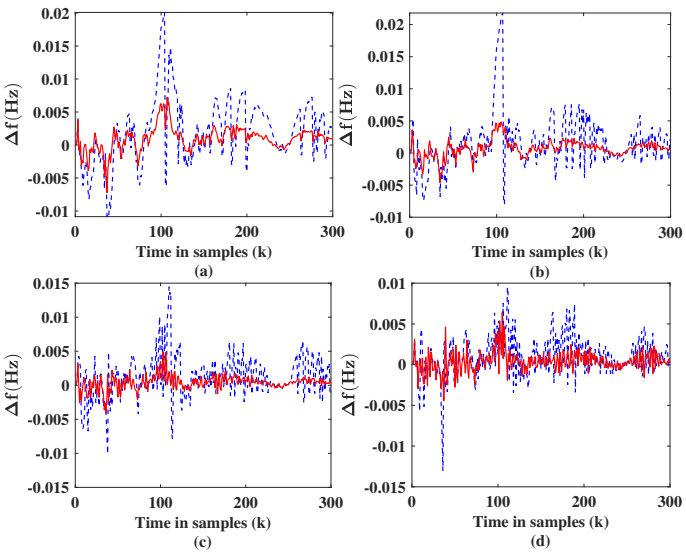

Fig. 5. Δf under different levels of intermittent feedback signals, the blue line indicates the conventional controller while the red line indicates the resilient controller. (a) $\bar{\vartheta} = 0.95, \bar{\varrho} = 0.95$. (b) $\bar{\vartheta} = 0.95, \bar{\varrho} = 0.85$. (c) $\bar{\vartheta} = 0.95, \bar{\varrho} = 0.75$. (d) $\bar{\vartheta} = 0.95, \bar{\varrho} = 0.65$.

Fig. 5 compares Δf with different intermittent transmission probabilities $1 - \bar{\varrho} = 0.05, 0.15, 0.25, 0.35$, while the intermittent measurement probability maintains $1 - \bar{\vartheta} = 0.05$. Table I gives the corresponding resilient control gains, respectively. In Fig. 5, it is obvious that the presented control approach can achieve smaller overshoot and faster convergence than the conventional controller when facing variant power from DRESs with different probabilities of intermittent feedback signals. According to Fig. 5, it is evident that the proposed control approach is capable of achieving superior frequency regulation dynamics, which verifies the efficacy of the proposed approach under different levels of intermittent feedback signals.

TABLE I
RESILIENT CONTROL GAINS UNDER $1 - \bar{\vartheta} = 0.05$

Intermittent transmission	Resilient controller gains
$1 - \bar{\varrho} = 0.05$	$[-1.3190 \quad 0.2993 \quad -0.0044 \quad -0.0646]$
$1 - \bar{\varrho} = 0.15$	$[-1.1546 \quad 0.2720 \quad -0.0577 \quad -0.0841]$
$1 - \bar{\varrho} = 0.25$	$[-0.9894 \quad 0.2471 \quad -0.0800 \quad -0.0709]$
$1 - \bar{\varrho} = 0.35$	$[-0.9177 \quad 0.2052 \quad -0.1312 \quad -0.0922]$

Similar to Fig. 5, Fig. 6 compares the frequency deviation dynamics under different intermittent transmission probabilities $1 - \bar{\varrho} = 0.10, 0.20, 0.30, 0.40$, while the intermittent measurement probability is fixed as $1 - \bar{\vartheta} = 0.15$. Table II gives the corresponding resilient control gains, respectively. The trend observed in Fig. 6 reaffirms the findings from Fig. 5. Specifically, the resilient controller demonstrates superior frequency regulation compared to the traditional controller across different probabilities of intermittent feedback signals. This trend also indicates that the proposed controller is capable of effectively mitigating the impact of load disturbances and wind power imbalance, maintaining better performance despite different probabilities of intermittent feedback signals.

TABLE II
RESILIENT CONTROLLER GAINS UNDER $1 - \bar{\vartheta} = 0.15$

Intermittent transmission	Resilient controller gains
$1 - \bar{\varrho} = 0.10$	$[-1.0336 \quad 0.2628 \quad -0.0492 \quad -0.0684]$
$1 - \bar{\varrho} = 0.20$	$[-0.9811 \quad 0.2376 \quad -0.1017 \quad -0.0805]$
$1 - \bar{\varrho} = 0.30$	$[-0.8343 \quad 0.1842 \quad -0.1306 \quad -0.0769]$
$1 - \bar{\varrho} = 0.40$	$[-0.5791 \quad 0.1955 \quad -0.0606 \quad -0.0370]$

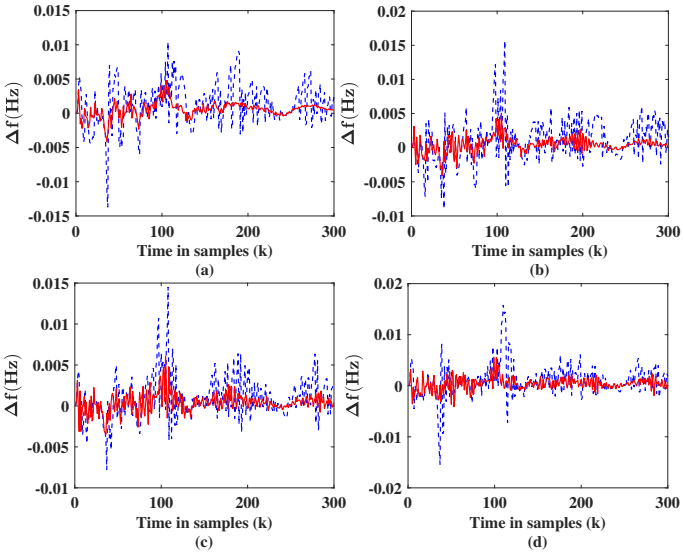

Fig. 6. Δf under different levels of intermittent feedback signals, the blue line indicates the traditional controller while the red line indicates the resilient controller. (a) $\bar{\vartheta} = 0.85, \bar{\varrho} = 0.90$. (b) $\bar{\vartheta} = 0.85, \bar{\varrho} = 0.80$. (c) $\bar{\vartheta} = 0.85, \bar{\varrho} = 0.70$. (d) $\bar{\vartheta} = 0.85, \bar{\varrho} = 0.60$.

V. CONCLUSION

The paper studied the resilient LFC problem considering intermittent feedback signals, including intermittent measurement and intermittent transmission, in the context of multiple

DRESs. To mitigate the impact of fluctuant power outputs from DRESs, robust performance index was incorporated in the control gains selection. The sufficient condition was deduced to ensure the mean-square stability for the system, from which the resilient control gains can be automatically determined. The validation results demonstrated that the frequency dynamic can be greatly enhanced with the participation of PEVs, and that the presented resilient frequency controller can well sustain the frequency dynamic under different levels of intermittent feedback signals.

REFERENCES

[1] L. Cristaldi, M. Faifer, C. Laurano, R. Ottoboni, E. Petkovski, and S. Toscani, "Power generation control algorithm for the participation of photovoltaic panels in network stability," *IEEE Transactions on Instrumentation and Measurement*, vol. 72, pp. 1–9, 2023.

[2] Y. Li, H. Zhang, X. Liang, and B. Huang, "Event-triggered-based distributed cooperative energy management for multienergy systems," *IEEE Transactions on Industrial Informatics*, vol. 15, no. 4, pp. 2008–2022, 2019.

[3] Z. Jiang and Y. Liu, "Low-voltage ride-through remote testing method for offshore wind turbines," *IEEE Transactions on Instrumentation and Measurement*, vol. 69, no. 6, pp. 2905–2913, 2020.

[4] Z. Hu, R. Su, K.-V. Ling, Y. Guo, and R. Ma, "Resilient event-triggered MPC for load frequency regulation with wind turbines under false data injection attacks," *IEEE Transactions on Automation Science and Engineering*, DOI: 10.1109/TASE.2023.3337006.

[5] S. Beura and B. P. Padhy, "Implementation of novel reduced-order H_∞ filter for simultaneous detection and mitigation of FDI-attacks in AGC systems," *IEEE Transactions on Instrumentation and Measurement*, vol. 72, pp. 1–12, 2023.

[6] P. Chen, D. Zhang, L. Yu, and H. Yan, "Dynamic event-triggered output feedback control for load frequency control in power systems with multiple cyber attacks," *IEEE Transactions on Systems, Man, and Cybernetics: Systems*, vol. 52, no. 10, pp. 6246–6258, 2022.

[7] C. Muscas, P. A. Pegoraro, S. Sulis, M. Pau, F. Ponci, and A. Monti, "New Kalman filter approach exploiting frequency knowledge for accurate PMU-based power system state estimation," *IEEE Transactions on Instrumentation and Measurement*, vol. 69, no. 9, pp. 6713–6722, 2020.

[8] Z. Gao, Y. Song, and C. Wen, "Asymptotic tracking control with bounded performance index for MIMO systems: A neuroadaptive fault-tolerant proportional-integral solution," *IEEE Transactions on Cybernetics*, DOI: 10.1109/TCYB.2023.3273229.

[9] G. Liu, H. Liang, Y. Pan, and C. K. Ahn, "Antagonistic interaction-based bipartite consensus control for heterogeneous networked systems," *IEEE Transactions on Systems, Man, and Cybernetics: Systems*, vol. 53, no. 1, pp. 71–81, 2023.

[10] Z. Gao, Y. Song, C. Wen, and F. L. Lewis, "Asymptotic output tracking with malfunctioning actuators and twisted/biased feedback," *IEEE Transactions on Systems, Man, and Cybernetics: Systems*, vol. 54, no. 3, pp. 1719–1729, 2024.

[11] D. S. Roy, C. Murthy, and D. K. Mohanta, "Reliability analysis of phasor measurement unit incorporating hardware and software interaction failures," *IET Generation, Transmission & Distribution*, vol. 9, no. 2, pp. 164–171, 2015.

[12] Z. Xu, D. Wang, G. Yi, and Z. Hu, "Asynchronous tracking control of amplitude signals in vibratory gyroscopes with partially unknown mode information," *IEEE Transactions on Industrial Electronics*, vol. 70, no. 7, pp. 7478–7487, 2023.

[13] P. Zhang, J. Zhang, J. Yang, and S. Gao, "Resilient event-triggered adaptive cooperative fault-tolerant tracking control for multiagent systems under hybrid actuator faults and communication constraints," *IEEE Transactions on Aerospace and Electronic Systems*, vol. 59, no. 3, pp. 3021–3037, 2023.

[14] K. Zhang, Z. Hu, F. Song, X. Yang, and Y. Liu, "Consensus of input constrained multi-agent systems by dynamic time-varying event-triggered strategy with a designable minimal inter-event time," *IEEE Transactions on Circuits and Systems II: Express Briefs*, vol. 71, no. 4, pp. 2119–2123, 2024.

[15] C. Murthy, A. Mishra, D. Ghosh, D. S. Roy, and D. K. Mohanta, "Reliability analysis of phasor measurement unit using hidden Markov model," *IEEE Systems Journal*, vol. 8, no. 4, pp. 1293–1301, 2014.

[16] G. Liu, Q. Sun, R. Wang, and X. Hu, "Nonzero-sum game-based voltage recovery consensus optimal control for nonlinear microgrids system," *IEEE Transactions on Neural Networks and Learning Systems*, vol. 34, no. 11, pp. 8617–8629, 2023.

[17] K. Ding, Q. Zhu, and T. Huang, "Partial-information-based non-fragile intermittent estimator for microgrids with semi-aperiodic DoS attacks: Gain stochastic float," *IEEE Transactions on Power Systems*, vol. 39, no. 1, pp. 2271–2283, 2024.

[18] Z. Hu, S. Liu, W. Luo, and L. Wu, "Resilient distributed fuzzy load frequency regulation for power systems under cross-layer random denial-of-service attacks," *IEEE Transactions on Cybernetics*, vol. 52, no. 4, pp. 2396–2406, 2022.

[19] K. Zhang, B. Zhou, M. Hou, and G.-R. Duan, "Practical prescribed-time stabilization of a class of nonlinear systems by event-triggered and self-triggered control," *IEEE Transactions on Automatic Control*, vol. 69, no. 5, pp. 3426–3433, 2024.

[20] T. Duan and V. Dinavahi, "Fast path recovery for single link failure in SDN-enabled wide area measurement system," *IEEE Transactions on Smart Grid*, vol. 13, no. 2, pp. 1645–1653, 2022.

[21] X. Zhao, S. Zou, and Z. Ma, "Decentralized resilient H_∞ load frequency control for cyber-physical power systems under DoS attacks," *IEEE/CAA Journal of Automatica Sinica*, vol. 8, no. 11, pp. 1737–1751, 2021.

[22] S. Liu, W. Luo, and L. Wu, "Co-design of distributed model-based control and event-triggering scheme for load frequency regulation in smart grids," *IEEE Transactions on Systems, Man, and Cybernetics: Systems*, vol. 50, no. 9, pp. 3311–3319, 2020.

[23] M. Landi and G. Gross, "Measurement techniques for online battery state of health estimation in vehicle-to-grid applications," *IEEE Transactions on Instrumentation and Measurement*, vol. 63, no. 5, pp. 1224–1234, 2014.

[24] S. Han, S. Han, and K. Sezaki, "Development of an optimal vehicle-to-grid aggregator for frequency regulation," *IEEE Transactions on Smart Grid*, vol. 1, no. 1, pp. 65–72, 2010.

[25] H. Yang, C. Y. Chung, and J. Zhao, "Application of plug-in electric vehicles to frequency regulation based on distributed signal acquisition via limited communication," *IEEE Transactions on Power Systems*, vol. 28, no. 2, pp. 1017–1026, 2013.

[26] J. Morel, H. Bevrani, T. Ishii, and T. Hiyama, "A robust control approach for primary frequency regulation through variable speed wind turbines," *IEEJ Transactions on Power and Energy*, vol. 130, no. 11, pp. 1002–1009, 2010.

[27] A. Hajizadeh and M. A. Golkar, "Intelligent power management strategy of hybrid distributed generation system," *International Journal of Electrical Power & Energy Systems*, vol. 29, no. 10, pp. 783–795, 2007.

[28] C.-F. Lu, C.-C. Liu, and C.-J. Wu, "Effect of battery energy storage system on load frequency control considering governor deadband and generation rate constraint," *IEEE Transactions on Energy Conversion*, vol. 10, no. 3, pp. 555–561, 1995.

[29] Z. Hu, S. Liu, W. Luo, and L. Wu, "Intrusion-detector-dependent distributed economic model predictive control for load frequency regulation with PEVs under cyber attacks," *IEEE Transactions on Circuits and Systems I: Regular Papers*, vol. 68, no. 9, pp. 3857–3868, 2021.

[30] Z. Gu, C. K. Ahn, D. Yue, and X. Xie, "Event-triggered H_∞ filtering for T–S fuzzy-model-based nonlinear networked systems with multisensors against DoS attacks," *IEEE Transactions on Cybernetics*, vol. 52, no. 6, pp. 5311–5321, 2022.